Arab J Geosci (2015) 8:7125–7139
DOI 10.1007/s12517-014-1673-7

ORIGINAL PAPER

Geology, geochemistry, sulfur isotope composition, and fluid inclusion data of Farsesh barite deposit, Lorestan Province, Iran

Samira Mokhtari Asl · Mohammadreza Jafari · Reza Zarei Sahamiyeh · Vahid Shahrokhi

Received: 15 July 2014 / Accepted: 7 October 2014 / Published online: 5 November 2014

Abstract Farsesh barite in the central part of Iranian Sanandaj-Sirjan zone is a sample of epigenetic hydrothermal mineralization in dolomitized limestone, which provides appropriate chemicophysical conditions making the passage of mineral-bearing fluids possible. Barite veins may range from a few centimeters to 2 m in thickness that increases downward. The microthermometry measurements obtained from more than 30 fluid inclusions show relative homogenization temperatures ranging from 125 to 200 °C with an average of 110 °C for Farsesh barite deposits. The mean salinity measured proves 16 times as much as weight percentage of NaCl for barite. Coexistence of liquid- and vapor-rich fluid inclusions in barite minerals may provide an evidence of boiling in ore veins. Moreover, occurrence of bladed calcite, high-grade ore zones, and presence of hydrothermal breccia are all consistent with boiling. Thermometric studies indicate that homogenization temperatures (Th) for primary and pseudosecondary fluid inclusions in barite range from 125 to 200 °C with an average of 1,100 °C. The $\delta^{34}S$ values of barite also lie between 8.88 and 16.6 %. The relatively narrow spread in $\delta^{34}S$ values may suggest uniform environmental conditions throughout the mineralization field. Thus, $\delta^{34}S$ values are lower than those of contemporaneous seawater, which indicates a contribution of magmatic sulfur to the ore-forming solution. Barite is marked by total amounts of rare Earth elements (REEs) (6.25–17.39 ppm). Moreover, chondrite-normalized REE patterns of barite indicate a fractionation of light REEs (i.e., LREEs) from La to Sm, similar to those for barite from different origins. The La_{CN}/Lu_{CN} ratios and chondrite-normalized REE patterns reveal that barite in Farsesh deposit is enriched in LREEs compared with heavy rare Earth elements (HREEs). Similarity between Ce/La ratios in barite samples and those found in deep-sea barite supports its marine origin. Lanthanum and Gd exhibit positive anomalies, which are common features of chemical marine sediments. Cerium shows a negative anomaly in most samples inherited from the negative Ce anomaly of hydrothermal fluid that is mixed with seawater at barite precipitation. The available data including tectonic setting, host rock characteristics, REE geochemistry, and sulfur isotopic compositions may support a hydrothermal submarine origin for Farsesh barite deposit.

Keywords Barite · Farsesh · Sulfur isotope · Fluid inclusion

S. M. Asl (✉) · M. Jafari
Department of Geology, North Tehran Branch, Islamic Azad University, Tehran, Iran
e-mail: Samira.mokhtari01@gmail.com

R. Z. Sahamiyeh
Department of Geology, Lorestan University, Khorramabad, Iran

V. Shahrokhi
Department of Geology, Khorramabad Branch, Islamic Azad University, Khorramabad, Iran

Introduction

The major constituents of barite are Ba^{2+} and S in its oxidized state $SO4^{2-}$. Although Ba and Sr are relatively abundant and widely distributed elements in Earth crustal rocks (Faure 1998), most naturally occurring fluids are undersaturated with respect to barite (Chow and Goldberg 1960; Church and Wolgemuth 1972; Monnin et al. 1999; Rushdi et al. 2000; Ehya 2012; Zhang et al. 2013). Thus, for barite to precipitate, interaction between distinct sources of Ba and SO_4 is necessary. Regarding barite, saturation should also be maintained for preserving the mineral after precipitation. Hydrothermal barite precipitates from Ba-rich fluids formed in association with hydrothermal volcanic activity ascending from depth and mixing with seawater near the seafloor. Extensional faults and fractures may direct hydrothermal fluids upward onto the seafloor, where they mix with seawater, the primary source of SO_4 for barite

precipitation. The main Ba source for hydrothermal fluids is due to oceanic or continental rocks' leaching driven by heat from magmatic activity. Hydrothermal leaching of pelagic sediments enriched in Ba is another potential source of Ba for these fluids (Murchey et al. 1987). Barite solubility decreases during the lowering of pressure at any temperature, and with decreasing temperature, below 100 °C (Hanor 2000). It further makes barite precipitation from hydrothermal solutions possible. The geochemistry of the hydrothermal fluid, as well as size and composition of barite deposit, is determined by the type and amount of host volcanic rocks and the sediments through which the fluid has passed (Hanor 2000). Hydrothermal fluid temperature is further distinguished in different environments where "hydrothermal" barite forms. Barite can precipitate from low-temperature (<120 °C) hydrothermal fluids around "warm springs" at the seafloor. Barite may also precipitate at average temperatures (150 to 250 °C) in hydrothermal settings of continental margins where fluid circulation due to high heat flow is common (Hein et al. 2007; and references therein). This mode of precipitation occurs at the seafloor near hydrothermal plumes and forms chimneys and mounds. It may also occur within the sediments as dispersed crystals in basement fractures at oceanic back-arc basin spreading centers, fracture zones, and volcanic arcs (e.g., East Pacific Rise 1 N, Huheey et al. 1993; Tonga arc, south-west Pacific, Stoffers et al. 2006; the Kurile and western Aleutian Island arcs, north-west Pacific, Glasby et al. 2006; Okinawa and Mariana Troughs, Japan (Luders et al. 2001; Noguchi et al. 2011). Barite deposits are widely distributed in Iran. Approximately, 100 small barite deposits/prospects occur throughout Iran with a total barite reserve of roughly 10 million tons (Ghorbani 2002). The largest barite deposits are found in the central Alborz and central Iran zones, hosted by dolomitic and volcano sedimentary rocks. Barite mineralization has already been studied in several works (Martin et al. 1995; Torres et al. 2003; Wagner et al. 2005; Taghipour et al. 2010; Feng and Roberts 2011; Ehya 2012; Zhang et al. 2013).

Farsesh barite deposit is located about 45 km southeast of Aligoudarz in Lorestan Province, southeastern Iran. The present work, however, offers the first detailed investigation into barite mineralization in Farsesh barite deposit through isotopic composition, rare Earth elements, fluid inclusion studies, along with field observations, to understand the conditions of barite formation.

Geological setting

Iran is geologically complex (Fig. 1) and located in the middle of the Alpine-Himalayan mountain system. The geology, particularly the tectonic evolution of Iran, was greatly influenced by the development of the Tethys region. The tectonic events that affected the Iranian plate were caused by the opening and closing of the Paleo-and Neo-Tethys Oceans (Berberian and King 1981; Stöcklin 1977). It is believed that the opening of the Paleo-Tethys Ocean in northern Iran has occurred during the Ordovician-Silurian period, followed by the northward subduction of its oceanic crust beneath the Turan plate in Late Devonian and Late Triassic-Jurassic collision between the Iranian microcontinent and Turan plates (Stampfli 2000; Natalin and Şengör 2005). Following the closure of the Paleo-Tethys Ocean, construction of the Neo-Tethys oceanic crust in southern Iran and its later subduction below the central Iran plate took place during late Jurassic to Cretaceous (Mohajjel et al. 2003; Richards et al. 2006).

Continuous subduction resulted in the consumption of the Neo-Tethys oceanic basin following the collision of the Iranian-Arabian plates during the Oligo-Miocene (Stöcklin 1977; Berberian and King 1981; Stampfli 2000). Therefore, based on the differences in the crustal characteristics and the age of basement consolidation, Iran is divided into three major structural units including from south to north: (1) the Zagros folded belt; (2) central Iran and the Alborz Mountains; and (3) the south Caspian depression and the Kopehdagh mountain range. These major zones are subdivided into subzones based on differences in structural style, age, and intensity of deformation, as well as age and nature of magmatism (Davoudzadeh 1997) (Fig. 1).

Farsesh region is located in Sanandaj–Sirjan tectono-metamorphic belt at the western margin of the Iranian central zone (Fig. 1) (Stöcklin 1977). A simplified geologic map of Farsesh area is shown in Fig. 1. The order of rock units from the oldest to youngest is as follows: metamorphic rocks including marble, weathered dolomite, and acidic-basic metavolcanic rocks (Precambrian-Cambrian); black shale with thin bands of sandstone and limestone (middle-late Devonian); Dolomitic limestone (carboniferous); and andesite-dacite volcanic sedimentary sequence and limestone (Eocene).

As a result, Eocene volcano sedimentary units are disconformably overlain by a red to brown, terrigenous unit of the Oligocene age. This unit is composed of conglomerate with intercalations of sandstone (Lower Red Formation).

The sequence is intruded by numerous acidic to intermediate volcanic tuffs of post-Eocene age of Farsesh barite in southeastern Aligoudarz. Igneous activity that occurred in Sanandaj-Sirjan metamorphic belt during Cenozoic period is due to the still continuous convergence of Afro-Arabian and Iranian plates (Stöcklin 1977).

Barite veins cut the dolomite and limestone units (Fig. 2a, b) and range from minute veinlet only a few centimeters in size to large veins more than 300 m long. The thickness also varies from a few centimeters up to 2 m. They trend in east-northeast and west-southwest, dipping steeply (65–800°) to the southeast.

Barite veins are composed of barite, quartz, and opaque (Fe-Ox) minerals (Fig. 2c–f). Barite is a predominant mineral and may comprise 90 % of the mineral constituents. There are two generations: an early large euhedral to subhedral generation of

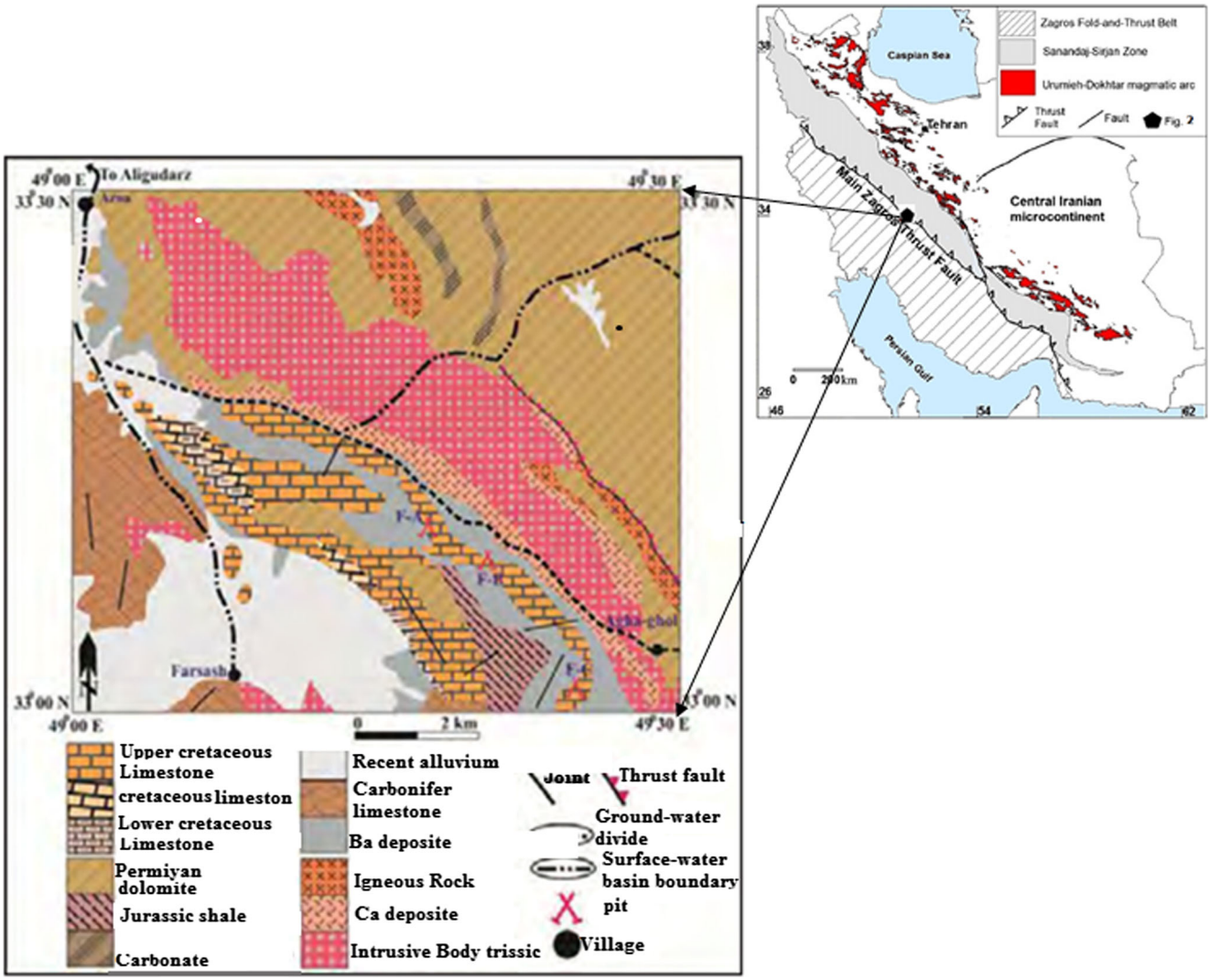

Fig. 1 Main tectonic elements of Iran and location of the simplified geologic map of the Farsesh barite deposit (modified after Stöcklin 1977)

crystals showing two perpendicular sets of cleavage and a later generation of anhedral crystals associated with quartz and opaque filling the interstitial spaces or cracks in the first generation. Quartz may form up to 30 % of total mineral constituents in some veins (Fig. 2c, d). It occurs as anhedral interstitial crystals replacing the edges of barite crystals and reflecting its later origin. Opaque minerals are dominated by Fe oxides (magnetite and specularite) with minor sulfides and a few disseminations of Au (Fig. 2e, f). Barite veins are associated with silicification of the host rocks in the form of secondary quartz, kaolinitization, and sericitization of the plagioclase.

Results and discussion

Sulfur isotopes

Sulfur isotopic data from barite deposits are useful for identifying the sources of sulfate and geochemical processes that act upon sulfate prior to its precipitation as barite. Variations in sulfur isotope compositions in natural systems result from different chemical exchange reactions and can be enhanced by bacterial reduction of sulfate (Hoefs and Sywall 1997; Seal et al. 2000). Sulfur isotopic signatures of marine and evaporated sulfate minerals have changed throughout geological time, providing a record of secular variations in seawater sulfate (Claypool et al. 1980). The $\delta^{34}S$ values of six samples from Farsesh barite deposit ores are shown in Table 1.

The S isotopic composition analyses were performed by EA-IRMS. Tin capsules containing reference or sample material plus vanadium pentoxide catalyst were loaded into an automatic sampler from which they were dropped in sequence into a furnace held at 1,080 °C and combusted in the presence of oxygen. These tin capsules flash combustion and increase the temperature in the region of the sample to ~1,700 °C. The combusted gases are then swept in a helium stream over combustion catalysts (tungstic oxide/zirconium oxide) and through a reduction stage of high-purity copper wires to

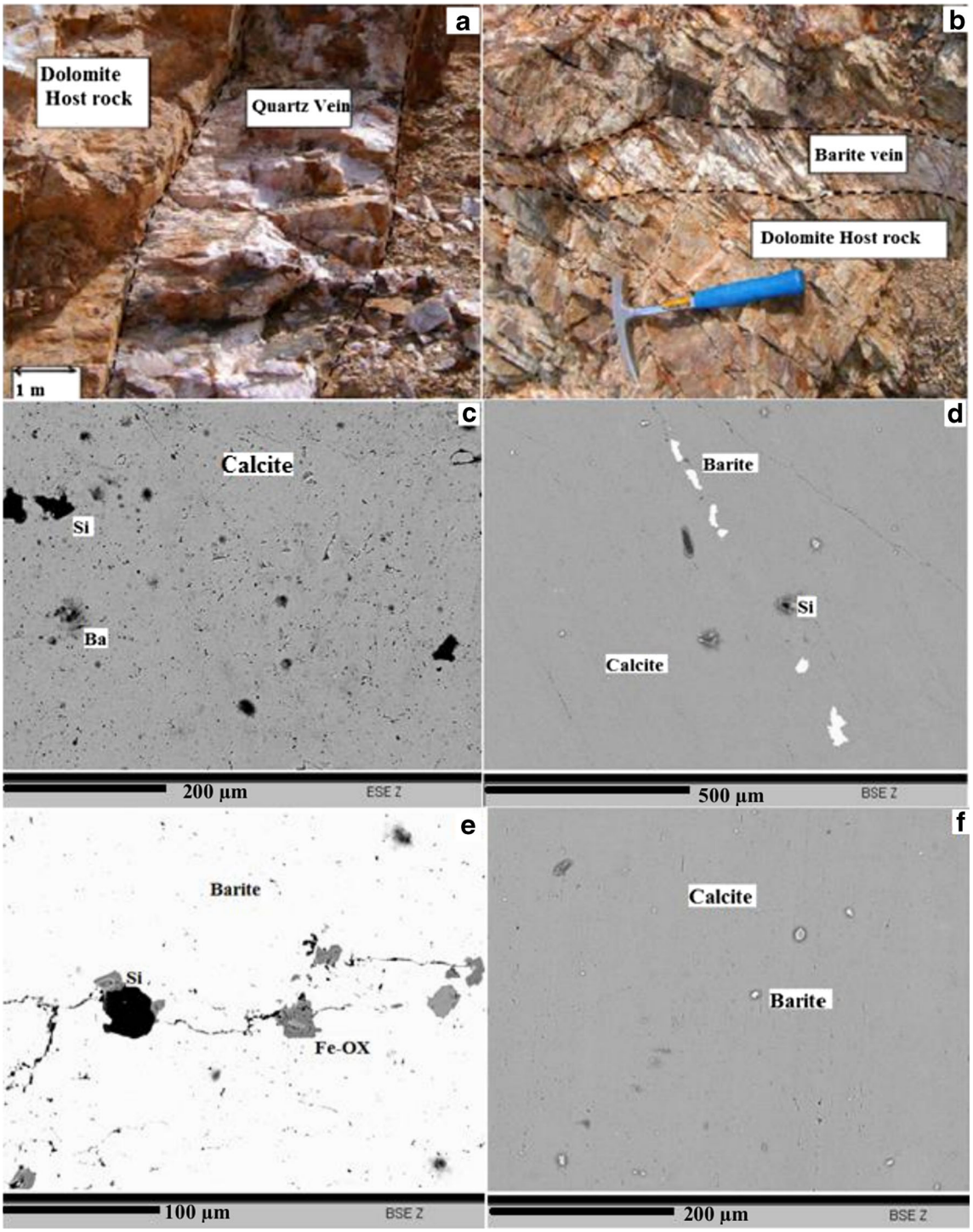

Fig 2 Ore occurrences and BSE images of Farsesh deposit. **a**, **b** Barite veins hosted by dolomitized limestone; **c**, **d** barite with calcite and silica; **e**, **f** occurrences of barite with Fe-Ox

produce SO_2, N_2, CO_2, and water. Then, water is removed using a Nafion™ membrane. Sulfur dioxide is resolved from N_2 and CO_2 on a packed GC column at a temperature of 45 °C. The resultant SO_2 peak enters the ion source of the IRMS whereupon it is ionized and accelerated. Gas samples of different mass are separated in a magnetic field, and simultaneously measured on a Faraday cup universal collector array. The analysis was based on monitoring of m/z 48, 49, and 50 of SO^+ produced from SO_2 in the ion source. The reference material used for analysis was IA-R061 (iso-analytical working standard barium sulfate, δ^{34}S-CDT=+20.33 ‰). IA-R025 (iso-analytical working standard barium sulfate,

Table 1 Sulfur isotope geochemistry from barites for Farsesh deposit

Sample no.	$\delta^{34}S$ (‰)
Far-S1	10.69
Far-S2	8.88
Far-S3	14.5
Far-S4	13.42
Far-S5	16.61
Far-S6	13.23

δ^{34}SV-CDT=+8.53 ‰), IA-R026 (iso-analytical working standard silver sulfide, δ^{34}SV-CDT=+3.96 ‰), and IA-R061 were used for calibration and correction of the 18O contribution to the SO+ion beam. Working standards are traceable to NBS-127 (barium sulfate, δ^{34}S-CDT=+20.3 ‰) and IAEA-S-1 (silver sulfide, δ^{34}SV-CDT=−0.3 ‰).

Analytical results show that $\delta^{34}S$ ranges from 8.88 to 16.6 ‰. Although Farsesh deposit is hosted by limestone and dolomite, they were formed epigenetically. When the S isotope results are compared with those of younger source materials, they are isotopically lighter than those of the Permian to Tertiary seawater sulfate $\delta^{34}S$=10–22 ‰ (Claypool et al. 1980) or barite from active hydrothermal vents, for instance, ($\delta^{34}S$=22 ‰) for barite from Mariana (Kusakabe et al. 1990). Although sulfur isotopic values in Farsesh deposit are lighter than those of Precambrian and Cambrian seawater (31 ‰) on the evaporitic sulfur isotope curve (Claypool et al. 1980), they are also much lighter than those of the Silurian and Devonian seawater (23–24 ‰). Light $\delta^{34}S$ values of Farsesh barite samples are inconsistent with $\delta^{34}S$ values of stratiform barite deposits from the Iglesiente-Sulcis mining district in Sardinia. The latter appear to be of epigenetic character (Cortecci and Frizzo 1993) and from late Proterozoic to lower Cambrian marine barite deposits of Liulin in Quinling Region and Xinghuang in Jiangnan Region of south China (Wang and Li 1991; Maynard and Okita 1991), deposited in a deep, poorly oxygenated, and tectonically active marine basin (Clark et al. 2004). The $\delta^{34}S$ values of Farsesh barite are heavier than those of Hüyük barite (a mean $\delta^{34}S$ value of 29.60 ‰), located in Sultandağ Region of the western Taurus mountains, assumed as stratiform barites with sedimentary and diagenetic features and their sulfate ions supplied from coeval seawater (Ayhan 2001).

As shown in Fig. 3, values of barite from Farsesh are consistent with those of contemporaneous seawater. The $\delta^{34}S$ values of barites (8.8–16.6 ‰) are lower than isotope values of contemporaneous seawater (22.0 ‰; Paytan et al. 2002). The $\delta^{34}S$ values of barite from high-temperature hydrothermal vents at modern volcanic arcs and back-arc basins match the value of modern seawater sulfate (21 ‰; Rees et al. 1978). On the other hand, Paytan et al. (2002) found modern marine barites of hydrothermal origin showing sulfur isotope values either equal to or lower than those of modern seawater. These hydrothermal barites formed when the circulating seawater leached Ba from the oceanic crust, then interacting and mixing with the sulfate-rich seawater (Kusakabe et al. 1990). Hydrothermal barite with very low values of $\delta^{34}S$ (mean 10.1 ‰), compared with seawater, was also reported by Goodfellow and Blaise (1988) from Middle Valley at the northern end of the Juan de Fuca Ridge. These low $\delta^{34}S$ values were interpreted as suggesting the derivation of a considerable sulfur proportion in the barite obtained from oxidation of dissolved H_2S or precipitated sulfide (Goodfellow and Blaise 1988). Thus, hydrothermal barites display a sulfur isotopic ratio equal to or lower than that of seawater depending on the relative contribution of magmatic sulfur derived from oxidation of H_2S (Hannington and Scott 1989). Lower values of $\delta^{34}S$ in barite from Farsesh deposit, if compared with those of seawater, are permissive of a similar process. Therefore, the sulfur involved in the formation of barite was not only exclusively derived from seawater sulfate, but also had a contribution of sulfur probably derived from magmatic H_2S oxidation.

Fluid inclusion studies

Sampling and methodology

Fluid inclusions were studied in doubly polished wafers of hydrothermal barite less than or equal to 150-μm thickness. Over 30 inclusions were measured for homogenization temperature (Th) and salinity determination. Homogenization temperatures (Th), as well as first-ice melting (Te) and last ice-melting (Tm ice) temperatures, were measured to obtain reliable data for microthermometry. Temperature determinations were performed three times for each inclusion. Microthermometry studies were conducted at the Department of Geology, Tarbiat Modarres University, Tehran, Iran. The stages were calibrated with a series of synthetic fluid inclusions of known compositions. The accuracy is ±10 °C on freezing. Salinities of liquid-rich fluid inclusions were calculated from the measured last ice-melting temperature using the equation offered by Hall et al. (1988).

Types and features of inclusions

As shown in Fig. 4a–d, three inclusion types were identified based on the number of phases observed at room temperature, degree of filling, and phase variations observed during the heating-freezing experiments: (I) liquid–vapor (L-V) (Fig. 4a, b), (II) liquid only (L) (Fig. 4c), and (III) vapor-only (V) inclusions (Fig. 4d). Type I and type II inclusions are two-phased (i.e., vapor and liquid). Type I inclusions are essentially vapor-rich and two-phased. They can be found in clusters or

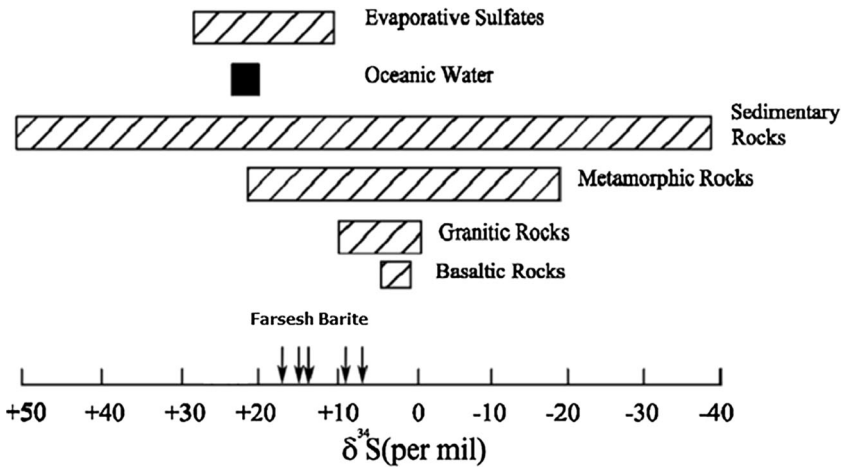

Fig. 3 Comparison on sulfur stable isotopes of the Farsesh barite deposits and other geological environments

sometimes isolated. These occurrences suggest a primary origin (Roedder 1984). In many cases, inclusions appear to contain one phase (e.g., vapor) at room temperature, although some involve a considerable amount of liquid. Type I inclusions contain a negative crystal shape and are usually small.

Type II inclusions are liquid-rich and two-phased, demonstrating slightly higher significant degree of filling than type I inclusions. The degree of filling may range from 0.3 to 0.6 (type I) and 0.5–0.9 (type II). Type II inclusions are considered primary, round, and faceted with an average size of 5*3 μm.

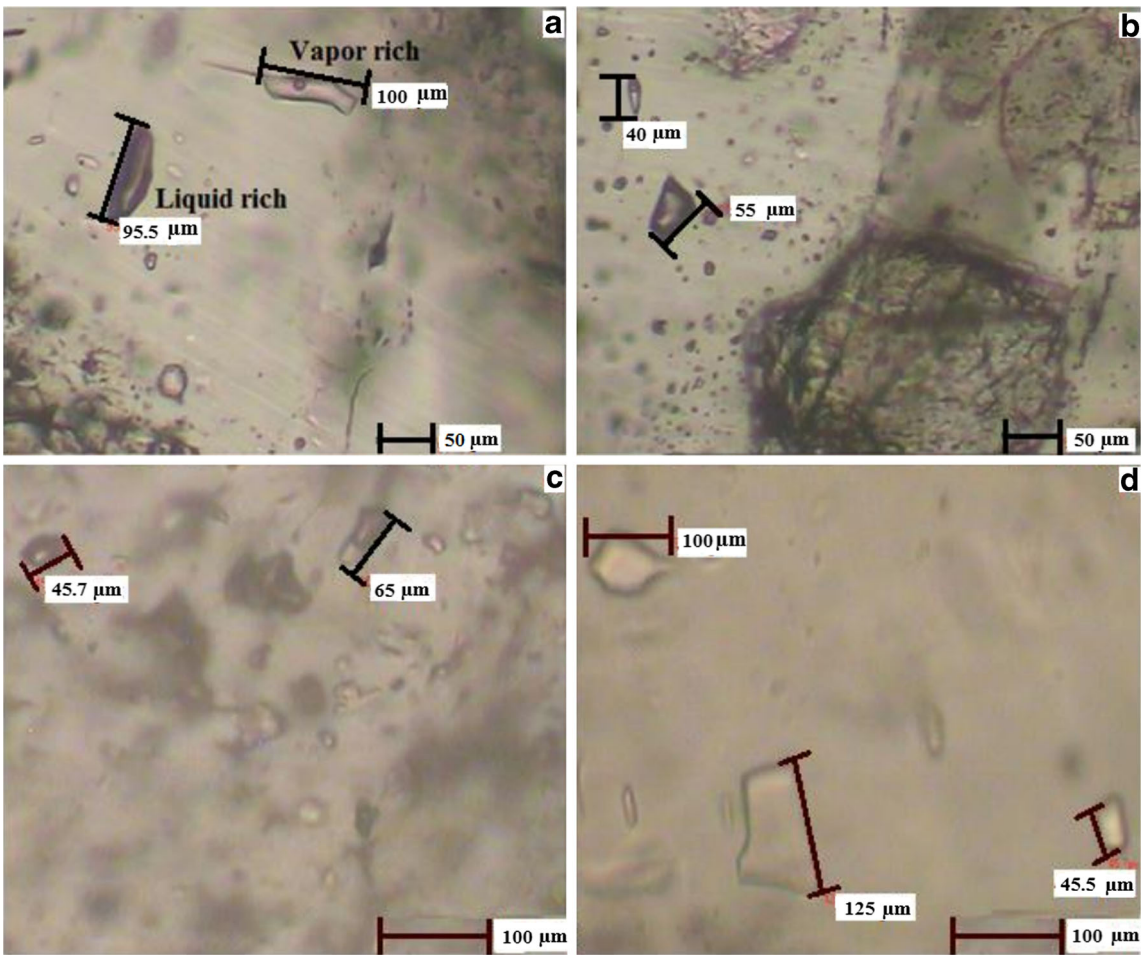

Fig. 4 Petrography and type of fluid inclusions from Farsesh barite deposit

Typically, inclusions less than 1 μm are not suitable for microthermobarometric measurements.

Type III inclusions are variable in size from 4*3 to 20*5 μm, having a relatively regular shape. In some cases, they occur in regular shapes as negative crystals. Type III inclusions occur as primary isolated inclusions, either along secondary or pseudosecondary trails. The degree of filling is 0.75–9.2.

Microthermometric measurements

Microthermometric analysis was conducted on primary and pseudosecondary LV fluid inclusions. Some secondary type III inclusions show a metastable ice in the absence of a vapor phase throughout the cooling of the first ice-melting occurred between −19 and −0.2 °C, indicating maximum salinities of 4–21 equiv.wt% NaCl, with an average of 16 wt.% NaCl (Fig. 5). Fluid inclusions with low salinity may indicate mixing of barite-bearing fluids and meteorite water.

Homogenization temperature data were analyzed for the inclusion hosted in barite minerals. Moreover, homogenization temperatures of fluid inclusion range from 125 to 200 °C with an average of 110 °C for barite. The stacking histogram clearly illustrates the frequency of homogenization temperature (Fig. 6) of 170 °C dominated by liquid-rich inclusions. There is no correlation between the size of inclusions and homogenization temperatures (Th). This shows that the results of homogenization temperature are more reliable, indicating the temperature of mineralization.

Homogenization temperatures versus salinity data for primary inclusions in barite minerals are plotted in Fig. 7. To understand the characteristics of hydrothermal fluids at Farsesh deposit, results have been compared with those of a few selected epigenetic hydrothermal barite deposits (Gultekin et al. 2003; Göke and Bozkaya 2008; Fuquan et al. 2006). High-salinity and high-temperature values of inclusions indicate a hydrothermal fluid of probable magmatic derivation circulated in Farsesh deposit (Arribas et al. 1995). The relatively high salinity (around 4–21 equiv. wt% NaCl), low-temperature 125–200 °C inclusions may be the result of episodic mixing of deep-saline brines of probable magmatic derivation with meteoric low-salinity fluids (Roedder 1984; Hedenquist et al. 1985; Arribas et al. 1995; Hill et al. 2000). The majority of Farsesh samples show salinity greater than 10 equiv.wt% NaCl. Moreover, with the exception of a few samples, most of them are homogenized between 150 and 200 °C. These inclusions in barite have some characteristics similar to epithermal barite mineralization. The relatively low-salinity and low-temperature inclusions are considered indicative of mixing magmatic and meteoric fluids.

In fluid inclusion types I, II, and III identified at Farsesh, there are different ranges of homogenization temperature and salinity (Fig. 9). Some type I inclusions have high homogenization temperatures, low-salinity values, and highly variable vapor/liquid ratios. The relationship between homogenization, temperature, and salinity of type I inclusions is not straightforward (Fig. 9), probably reflecting that these inclusions were trapped under boiling conditions. Specifically, in a single sample, the inverse relationship between Th and salinity is consistent with the boiling fluid process and steam loss.

The fluid related to epithermal mineralization at Farsesh is probably represented by type II inclusions. This fluid type is also partly responsible for hydrothermal alteration. The high salinity (from 11.6 to 17.5 equiv.wt% NaCl) and lower temperatures (from 142 to 167 °C) of type II inclusions record the late-stage hydrothermal fluid responsible for barite deposition. The low vapor-phase-bearing inclusions in barite crystals may suggest a deficiency that these inclusions are probably trapped close to boiling conditions (Fig. 9). On heating, high homogenization temperatures measured in type I inclusions of barite (from 171 to 200 °C, averaging 181.75 °C) (Figs. 8 and 9) indicate that these barites are related to magmatic type.

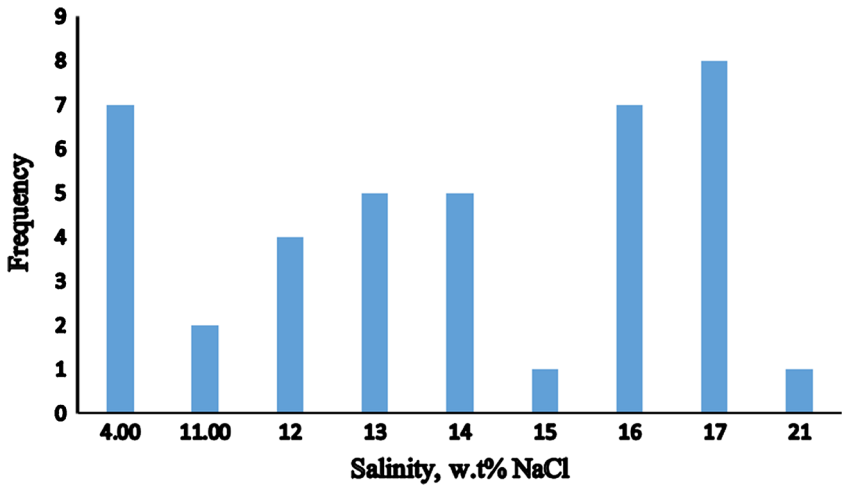

Fig. 5 Fluid inclusion salinities within barite minerals from Farsesh deposit

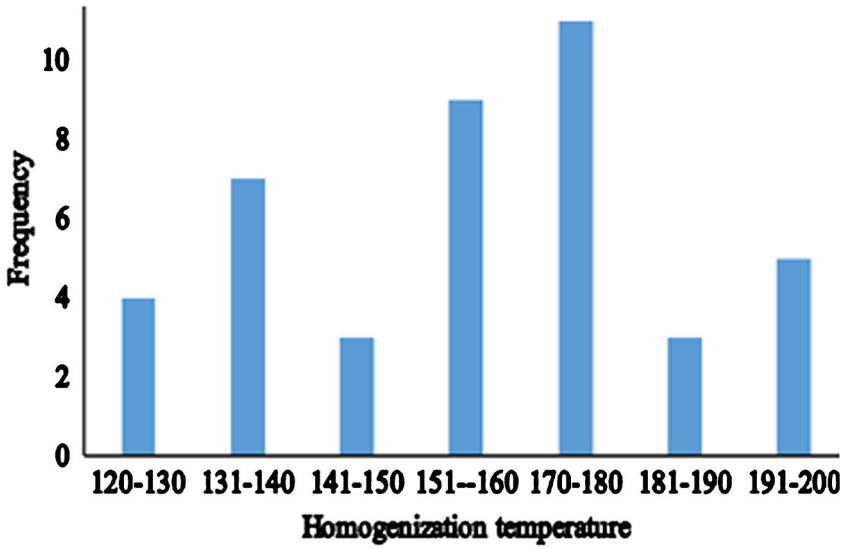

Fig. 6 Homogenization temperatures of fluid inclusions analyzed during this study

Geochemistry of rare Earth elements

Because of their unique geochemical characteristics, rare Earth elements (REEs) play a major role in understanding chemical evolution and material sources of hydrothermal fluids. Results of REE analysis are shown in Table 2. These results were normalized using the average C1 chondrite abundance of Boynton (1984). Such normalization is more commonly used in literature for studying REE distribution in barite. La and Gd anomalies were calculated as $(La/La^*)_{CN}=La_{CN}/(3Pr_{CN}-2Nd_{CN})$ and $(Gd/Gd^*)_{CN}=Gd_{CN}/(0.33Sm_{CN}+0.67Tb_{CN})$, respectively. On the other hand, to discriminate between real and apparent Ce anomalies (Bau et al. 1996; Shields et al. 2004; Ehya 2012), $(Ce/Ce^*)_{SN}$ and $(Pr/Pr^*)_{SN}$ ratios were calculated as $Ce_{SN}/(0.5La_{SN}+0.5Pr_{SN})$ and $Pr_{SN}/(0.5Ce_{SN}+0.5Nd_{SN})$, respectively. The suffix "SN" refers to the normalization of concentrations against the standard Post-Archean Australian Shale (PAAS; McLennan 1989). Most barite deposits in continental and deep water may indicate lower total REE concentration and positive Eu anomalies.

The REE patterns of normalized chondrite for barite samples are shown in Fig. 10, where the data have a similar pattern indicating that their formation has been through the same process; they have been enriched in LREEs and depleted in HREEs. Light rare Earth element (LREE) patterns in barite may help to determine depositional environments due to variations of LREE behavior in different hydrothermal environments (Guichard et al. 1979). REE substitution in barite structure causes LREE concentration in barite, because their ionic size is more similar to that of Ba^{2+} when compared with heavy rare Earth elements (HREEs) (Guichard et al. 1979). LREE data for barite, especially La_{CN}/Ce_{CN}, have been used to support biogenic sources for barite in some deposits in China (Wang and Li 1991) and in Nevada (Jewell and Stallard 1991). The La_{CN}/Lu_{CN} ratios of barite range from 3.05 to 47

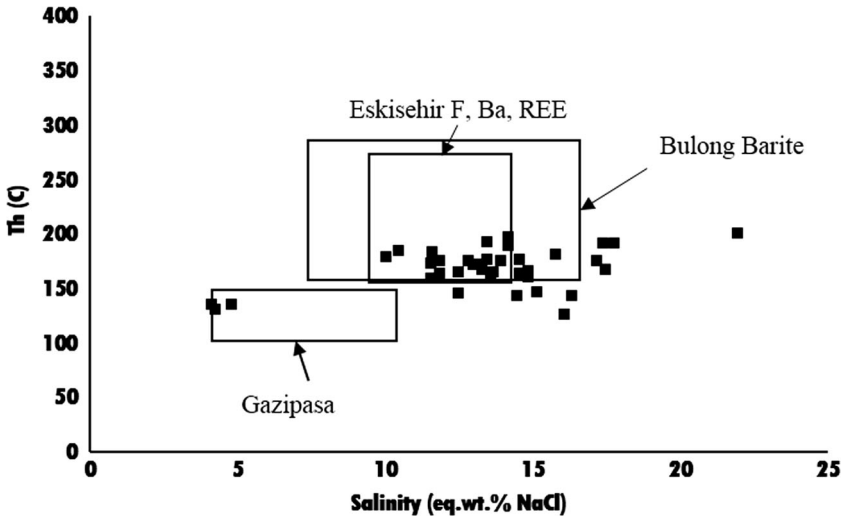

Fig. 7 Compression of homogenization temperature (T_h) versus salinity for primary fluid inclusions contained in Farsesh barite with other barite deposits

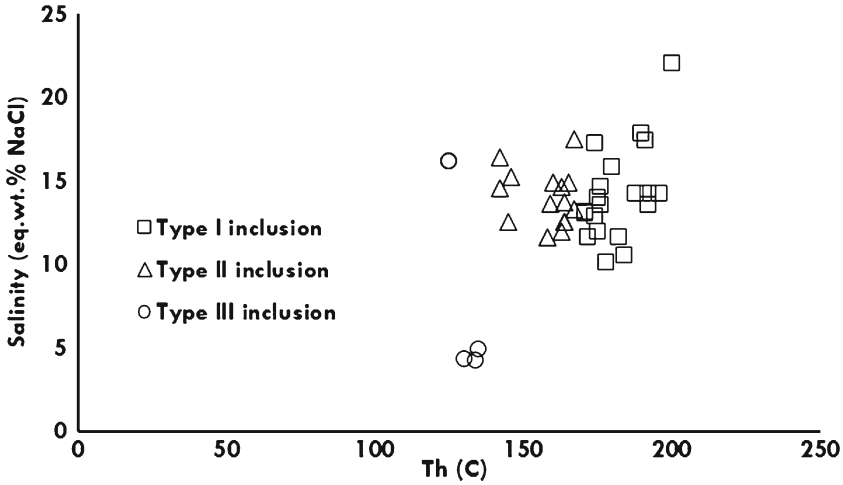

Fig. 8 Salinity versus homogenization temperatures (T_h) plot of different types of fluid inclusions

(Table 2). These ratios also indicate that barite is LREE-enriched relative to HREE. Since seawater has a typical LREE-depleted pattern, the LREE-enriched patterns observed in some marine precipitates result from a deposition in those marine environments with large inputs of hydrothermal vent fluids (Chen et al. 2006). Therefore, regardless of crystallographic limitations for HREE substitution in barite lattice, the LREE-enriched patterns of barite samples may reflect the probable existence of active hydrothermal vents near the place where barite was deposited.

The Ce/La ratios in barites were recognized by Guichard et al. (1979) as a discriminating factor to distinguish between marine and terrestrial barites. The Ce/La ratios in deep-sea barite are less than 1 and similar to those of seawater, while this ratio in terrestrial (vein) barite is greater than 1 and similar to that for basic rocks and clays (Guichard et al. 1979). The samples of barite analyzed here, which display Ce/La ratios ranging from 0.28 to 0.53 with an average of 0.41 (Table 2), are similar to marine barite. Furthermore, all the samples display $(La/La^*)_{CN}$ and $(Gd/Gd^*)_{CN}$ above unity, i.e., the features that are considered as those in marine chemical sediments regardless of their ages (Alexander et al. 2008).

Fluvial and continental shelf LREE waters characteristically show no pronounced depletion of Ce relative to other REEs. However, in oxygenated deep-ocean waters, the preferential removal of Ce results in a large negative anomaly (Guichard et al. 1979). The pattern is promoted by preferential scavenging of Ce from the water column by hydrothermally produced Mn and Fe oxides. It may result in hydrothermally influenced seawater with a negative Ce anomaly more extreme than that of which can be found elsewhere in seawater (Klinkhammer et al. 1983). Cherts from continental margin, together with pelagic and ridge-proximal depositional environments, have distinct LREE signatures independent of diagenetic modification (Murray 1994). The distinctive feature is the behavior of Ce relative to neighboring light LREEs (e.g., La, Pr, and Nd). Following the usage of Murray (1994), these behaviors are expressed as La_{CN}/Ce_{CN}, normalized against the "North American shale composite" of Gromet et al. (1984). The Ce/Ce* values in the open seawater and related deposits are less

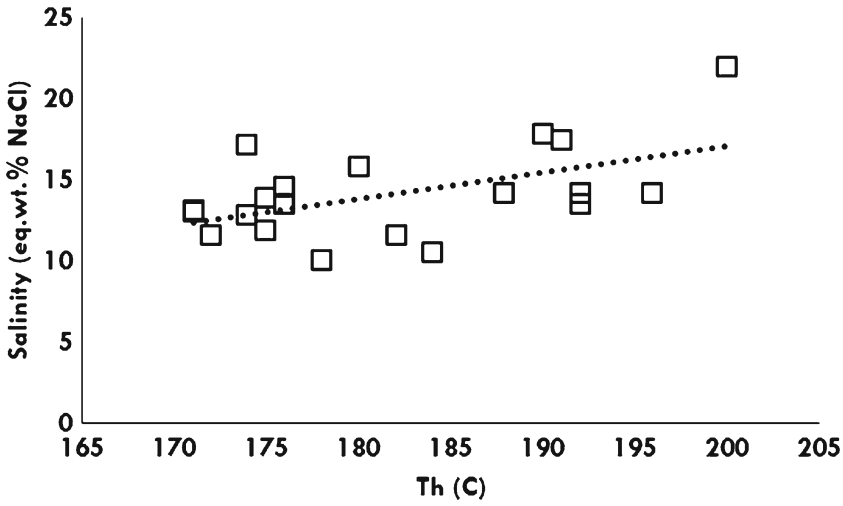

Fig. 9 Trend plot of the increasing or decreasing salinity along with temperature reduction

Table 2 Trace and rare Earth element composition (ppm) of barite samples analyzed

Sample	FS-12	FS-13	FS-26	FS-28	FS-29	FS-34	FS-41	FS-42	FS-43	FS-45
Rb	0.3	0.3	0.3	0.4	0.1	0.2	0.1	0.3	0.2	0.3
Sr	21,000	10,000	15,100	17,600	11,200	19,700	17,800	14,300	14,500	12,700
Zr	1.2	1.8	1.7	1.9	1.4	1.5	1.3	0.9	1.56	2.1
Y	1.3	2.1	3.1	1.6	1.2	1.7	1.5	1.4	1.6	1.8
Hf	1.2	0.9	1.23	0.9	1.85	1.67	1.4	1.5	1.4	0.9
Ta	2.6	1.9	2.1	3.1	2.9	1.6	2.8	3.4	2.9	2.7
la	18.1	15.3	17.6	15.4	19.2	17.6	15.4	16.3	15.4	19.2
Ce	8.1	8.1	7.6	4.6	7.6	4.9	5.9	7.5	6.4	8.5
Pr	0.32	0.41	0.51	0.21	0.36	0.45	0.64	0.84	0.42	0.71
Nd	0.45	0.41	0.51	0.42	0.51	0.62	0.31	0.42	0.51	0.43
Sm	0.26	0.31	0.43	0.29	0.31	0.43	0.31	0.29	0.42	0.31
Rb	0.84	0.71	0.82	0.81	0.64	0.76	0.81	0.71	0.76	0.81
Eu	2.15	2.31	3.25	3.26	3.14	2.67	3.2	2.67	3.35	3.17
Gd	1.75	1.54	1.76	1.81	1.64	1.72	1.64	1.82	1.64	1.79
Ga	0.05	0.04	0.04	0.04	0.03	0.029	0.054	0.06	0.04	0.05
Ho	0.15	0.2	0.12	0.13	0.15	0.17	0.15	0.15	0.2	0.17
Tb	0.19	0.18	0.18	0.16	0.19	0.18	0.18	1.21	0.21	0.19
Er	0.25	0.34	0.22	0.26	0.34	0.28	0.25	0.25	0.28	0.24
Tm	0.04	0.04	0.042	0.05	0.4	0.038	0.05	0.04	0.04	0.037
Yb	0.16	0.11	0.13	0.19	0.09	0.04	0.19	0.11	0.09	0.14
Lu	0.04	0.04	0.05	0.4	0.5	0.6	0.4	0.4	0.05	0.05
∑REE	32.85	30.04	33.26	28.03	35.10	30.49	29.48	32.77	29.81	35.80
Ce/La	0.45	0.53	0.43	0.30	0.40	0.28	0.38	0.46	0.42	0.44
Y/Ho	8.7	10.5	25.8	12.3	8.0	10.0	10.0	9.3	8.0	10.6
La_{CN}/Lu_{CN}	47.00	39.73	36.56	4.00	3.99	3.05	4.00	4.23	31.99	39.89
$(La_{CN}/Lu_{CN})^*$	9.17	5.66	5.24	13.20	8.66	6.31	3.38	2.73	5.76	3.86
$(Gd_{CN}/Gd_{CN})^*$	18.06	13.90	11.90	16.52	14.78	11.69	14.64	31.57	11.90	15.88
$(Ce_{SN}/Ce_{SN})^*$	0.40	0.46	0.37	0.27	0.35	0.24	0.31	0.36	0.36	0.37
$(Pr_{SN}/Pr_{SN})^*$	0.63	0.82	1.05	0.68	0.74	1.28	1.74	1.78	1.00	1.35

than 1 and, in most cases, less than 0.5 (Shimizu and Masuda 1977; Elderfield 1988; Ding and Zhong 1996; Ehya 2012). This ratio for barite from Farsesh deposit ranges from 0.24 to 0.46, with an average of 0.35. Therefore, it appears likely that the negative Ce anomalies in these samples are inherited from seawater at their precipitation time. Hence, very low Ce anomalies of the studied barites provide further evidence that hydrothermal processes significantly contribute to their formation.

The Y/Ho ratio of seawater is more elevated (Y/Ho=101; Bao et al. 2008) than its chondritic ratio (Y/Ho=28; McDonough and Sun 1995). The hydrothermal vent fluids associated with mid-ocean ridges and back-arc basins have Y/Ho ratios ranging from 51 to 160 (Douville et al. 1999; Bao et al. 2008).

The Y/Ho ratios in hydrothermal vent fluids are not primarily controlled by mixing with seawater, but by the REE+Y (REY) uptake from them onto Fe, Mn-oxyhydroxides through coprecipitation with the particulate matter and scavenging (Bao et al. 2008). On the other hand, the REY patterns of chemical precipitates may differ from those of contemporaneous seawater due to the exchange effects between the REY scavenging particles and seawater, or the presence of detrital aluminosilicates (Alexander et al. 2008). For example, seafloor Fe-Mn crusts and Fe-oxyhydroxides precipitated from terrestrial spring water (Bau et al. 1998) display REY patterns in which Y/Ho ratios are lower than those of the host fluids (Alexander et al. 2008). This Y-Ho fractionation was attributed by Bau et al. (1996, 1998) to preferential adsorption of Ho relative to Y on Fe-Mn particles. The barite from Farsesh deposit exhibits Y/Ho ratios (8–25.8) considerably lower than those of seawater, hydrothermal vent fluids, and even chondrite. Therefore, subchondritic Y/Ho ratios of barite samples may reflect the negligible preferential adsorption of Y over Ho in barite lattice.

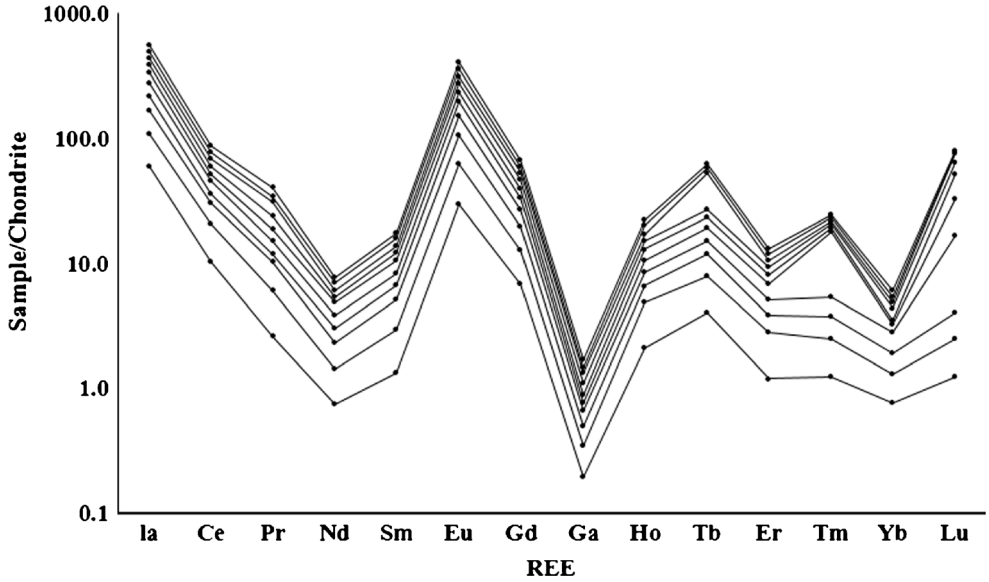

Fig 10 Plot of rare Earth elements (REEs) normalized to C1 chonderite McDonough and Sun (1995)

There is little data in the literature concerning the significance of Y/Ho ratio of barite. Thus, it is not possible to evaluate the importance of this ratio as a discriminating feature for barite from different origins. The barite from vein- and metasomatic-type of Duboki Vagan deposit in Bosnia possesses Y/Ho ratios of 3.44 and 5.21 (n=2) (Jurković et al. 2011). These ratios are slightly lower than those of barite from Farsesh deposit, indicating that terrestrial (vein) barite has apparently lower Y/Ho ratios than marine barite.

Most barite deposits possess chondrite-normalized REE patterns with Eu anomaly (Bernd and Paul 1996). In barite samples, Eu anomaly indicates minor differences due to evaluation of hydrothermal ore-bearing fluids with different temperatures. This difference is probably the result of mixing two fluids with different temperatures and oxygen fugacity, which is consistent with the data from microthermometry studies. Minor element contents of barite-rich rocks generally illustrate low Mn, Pb, and Zn concentrations and locally elevated Cu (0.3 wt.%), Au (0.5 ppm Au), Sb (26 ppm), and As content (38 ppm) (Table 2). Exceptionally high Sr values of barite-rich rocks are due to Sr^{2+} substitution in barite.

Origin and genetic model of Farsesh barite

Barite in submarine hydrothermal systems occurs as two principal end-member types: Submarine volcanic hydrothermal deposits directly associated with volcanic rocks, and sedimentary exhalative (sedex) deposits, mostly showing little spatial relationship with igneous rocks (Hanor 2000). In volcanic-hosted deposits, barite occurs in the ones with low concentrations of sulfides. In both ore types, Ba is leached from the source rocks in the oceanic crust by convective circulation of seawater (Hanor 2000). Supporting features for a submarine hydrothermal origin of barite in Farsesh deposit are the following: (1) The presence of dark-colored fossiliferous and carbonaceous strata within the footwall and hanging-wall rock units reveal that barite deposition has occurred in a marine sedimentary environment; (2) at the time of footwall rocks deposition, volcanic processes were active in sedimentary basin as evidenced by the presence of tuffs and lavas within the Eocene rocks; (3) open-space filling textures of barite and calcite reveal the deposition of these minerals by hydrothermal activities; (4) low ∑REE concentrations, LREE-enriched chondrite-normalized REE patterns, extremely low Ce anomalies, low Ce/La ratios, and positive La and Gd anomalies of barite are commonly considered as particular features of marine precipitates (including barite) deposited from hydrothermally influenced seawater (Guichard et al. 1979; Jewell and Stallard 1991; Chen et al. 2006; Alexander et al. 2008; Jurković et al. 2011); (5) sulfur isotope data are also consistent with deposition of barite from hydrothermal fluid entrained in seawater; and (6) studying the fluid inclusion of Farsesh mineralization may put constraints on the origin and evolution of the ore-forming fluid. Highly variable liquid–vapor ratios in primary fluid inclusions hosted by barite with two modes of 150 to 250 °C indicated that the barite was deposited from more heated fluids under boiling conditions. Igneous heat source in basement rocks may still prove the hydrothermal origin of Farsesh barite. It seems likely that the ore solutions that arrived in pulses and episodic nature of hydrothermal processes are supported by paragenetic evidence.

Based on these features, it is suggested that there were active submarine hydrothermal vents in Sanandaj-Sirjan zone during late Eocene. The hydrothermal fluids escaping from the vents carried sufficient barium to precipitate barite locally. As in the case for barite deposits associated with volcanic rocks, hydrothermal fluids acquired barium during the

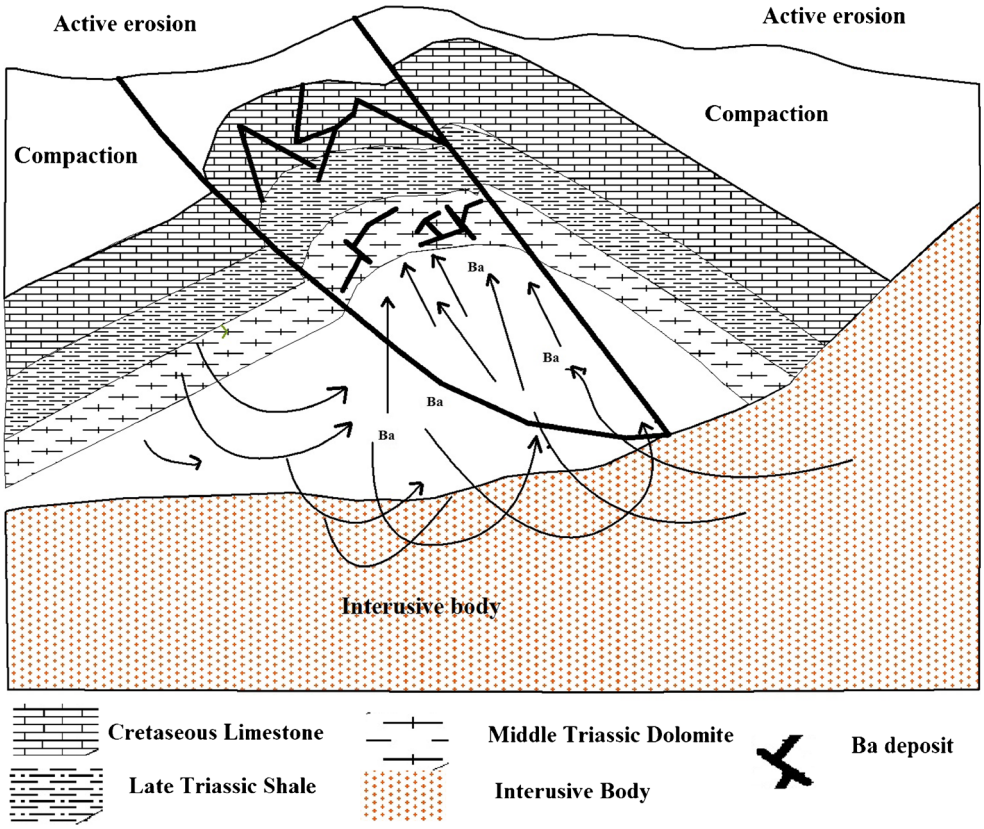

Fig. 11 Scheme of mineralization at Farsesh deposit. Basinal brine expulsion and deposition of barite ore along faulted and brecciated zones by hot mineralizing solutions

circulation of seawater in underlying volcanic source rocks. Barite deposition occurred on the seafloor where ascending hydrothermal barium-bearing fluids encountered sulfate-bearing marine waters in a manner similar to that found in modern analogs on the ocean floor.

The source of barium is important in developing a genetic model for Farsesh deposit. It is proposed that the presence of 100-ppm Ba in the formational waters is enough for a large amount of barite deposition (Kesler 1977). The albitization and diagenetic destruction of K-feldspar, mica, and clay in shale can release sufficient amounts of Pb, Zn, F, and Ba into the ore fluids of hydrothermal deposits (Liaghat et al. 2000). Clay mineral maturation and dewatering of shale may also provide Mg for dolomitization (Ghazban et al. 1994), and the liberated Ca^{+2} during dolomitization is consumed at barite formation. It should be noted that basinal brines are not generally rich in barite. Therefore, in most barite deposits, igneous activities can increase barite concentration of basinal brines (Ruiz et al. 1985). Based on the model presented here, a large-scale fluid flow through sedimentary rocks occurred in Farsesh deposit. On the deposit scale, mineralization tends to occur in breccias, and solution-collapse features are formed during the faulting process. Brecciation and faulting make the upward migration of ore fluids possible. The ore solutions had a remarkable ability to dissolve carbonate rocks. In the studied area, the NW-SE trending faults control the heat flux and act as channel ways for hot fluids. Heat may have been locally generated from deep-seated intrusions or volcanic flows, forcing the overlying pore fluids into convection. The leaching of some elements from andesitic rocks through alteration processes may increase the concentration of elements in the ore fluids (Fig. 11). Barite hydrothermal veins in the studied area contain at least 500 ppm Ba (Latifi 2000). It seems highly probable that some barites are originated from the phlogopite and biotite in igneous rocks (Valenza et al. 2000). The ore fluids do not rule out the possibility of a small magmatic component, or a higher temperature exchange between ore fluids and igneous rocks. However, if magmatic fluids were present, they might well mix with the formational water before reaching the site of ore deposition. The wide range of salinity is explained by mixing with meteoric water. Sulfur isotopic measurements of barite with high $\delta^{34}S$ values, alongside fluid inclusion data, show that these fluids do not resemble magmatic ones.

Conclusion

Mineralization at Farsesh deposit in Aligoudarz region is hosted by Permian dolomitized limestone. The paragenetic

sequence indicates that mineralization is entirely epigenetic. The mineralizing fluids are forced from orogens and squeezed out of the basin by crustal thickness and convergence in the studied area during Cenozoic orogeny. Fluid inclusion data indicate that the boiling that occurred at Farsesh deposit may have been an important mineralization mechanism for Ba. Coexisting liquid-rich and vapor-rich fluid inclusions in barite minerals may provide ample evidence for boiling in the ore veins. Mixing between magmatic water fluids and meteoric water has also been significant for ore deposition in Farsesh. In chondrite-normalized REE patterns, an LREE fractionation trend from La to Sm is similar to that reported for different types of barite. The chondrite-normalized REE patterns and La_{CN}/Lu_{CN} ratios reveal that barites are enriched in LREE compared with HREE. The Ce/La ratios as well as positive La and Gd anomalies are similar to those of marine precipitates and provide evidence to support a marine origin for barite. Negative Ce anomalies were probably inherited from hydrothermal fluid entrained in seawater at barite precipitation time. The $\delta^{34}S$ values of barites are lower than those of contemporaneous seawater, suggesting the involvement of magmatic sulfur derived from oxidation of H_2S in barite-forming solutions. Sulfur isotope values of barites indicate that they resemble the isotope compositions of barite formed from hydrothermal vents in modern volcanic arcs. Tectonic setting, host rock characteristics, REE geochemistry, and isotopic sulfur compositions are compatible with a submarine hydrothermal origin for barite in Farsesh deposit. Barite on the seafloor that has been formed from the ascending hydrothermal barium-bearing fluids encountered the seawater. Sulfate was derived from sulfate-bearing marine waters with the contribution of magmatic sulfur.

References

Alexander BW, Bau M, Andersson P, Dulski P (2008) Continentally-derived solutes in shallow archean seawater: rare earth elements and Nd isotope evidence in iron formation from the 2.9 Ga Pongola supergroup, South Africa. Geochim Cosmochim Acta 72:378–394

Arribas AJR, Cunningham CG, Rytuba RO, Kelly WC, Podwysocki MH, McKee EH, Tosdal RM (1995) Geology, geochemistry, fluid inclusion and isotope geochemistry of the Rodalquilar Au alunite deposits. Spain Econ Geol 90:795–822

Ayhan A (2001) Stratiform barite deposits between Sarkikaraagac (Isparta) and Huyuk (Konya) in Sultandag region, Turkey. Chem Erde-Geochem 61(1):54–66

Bao SX, Zhou HY, Peng XT, Ji FW, Yao HQ (2008) Geochemistry of REE and yttrium in hydrothermal fluids from the endeavour segment, Juan de Fuca Ridge. Geochem J 42:359–370

Bau M, Koschinsky A, Dulski P, Hein JR (1996) Comparison of the partitioning behaviors of yttrium, rare earth elements, and titanium between hydrogenetic marine ferromanganese crusts and seawater. Geochim Cosmochim Acta 60:1709–1725

Bau M, Usui A, Pracejus B, Mita N, Kanai Y, Irber W, Dulski P (1998) Geochemistry of low-temperature water-rock interaction: evidence from natural waters, andesite, and iron-oxyhydroxide precipitates at Nishiki-numa iron-spring, Hokkaido, Japan. Chem Geol 151:293–307

Berberian M, King GCP (1981) Towards a paleogeography and tectonic evolution of Iran. Can J Earth Sci 18:210–265

Bernd GL, Paul MA (1996) Geochemistry and exploration significance of ironstones and barite-rich rocks in the Proterozoic Willyama supergroup, olary block, South Australia. J Geochem Explor 57: 57–73

Boynton, WV (1984) Geochemistry of the rare earth elements: Meteorite studies. Henderson, P. (ed). Rare Earth Element Geochemistry. Elsevier

Chen D, Qing H, Yan X, Li H (2006) Hydrothermal venting and basin evolution (Devonian, South China): constraints from rare earth element geochemistry of chert. Sediment Geol 183:203–216

Chow TJ, Goldberg ED (1960) On the marine geo-chemistry of barium. Geochim Cosmochim Acta 20:192–198

Church TM, Wolgemuth K (1972) Marine barite saturation. Earth Planet Sci Lett 15:35–44

Clark RG, Hobson KA, Nichols JD, Bearhop S (2004) Avian dispersal and demography: scaling up to the landscape and beyond. Condor 106(4):717–719

Claypool GE, Holser WT, Kaplan IR, Sakai H, Zak I (1980) The age curves of sulfur and oxygen isotopes in marine sulfate and their mutual interpretation. Chem Geol 28:199–260

Cortecci G, Frizzo P (1993) Origin of siderite deposits from the Lombardy Valleys, northern Italy: a carbon, oxygen and strontium isotope study. Chem Geol 105(4):293–303

Davoudzadeh M (1997) Iran. In: Moores EM, Fairbridge RW (eds) Encyclopedia of European and Asian regional geology. Chapman & Hall, London, pp 384–405

Ding L, Zhong D (1996) Characteristics of rare earth elements and cerium anomalies in cherts from the Paleo-Tethys in Changning-Menglian belt in western Yunnan China. Sci China (Ser D) 39:35–45

Douville E, Bienvenu P, Charlou JL, Donval JP, Fouquet Y, Appriou P, Gamo T (1999) Yttrium and rare earth elements in fluids from various deep-sea hydrothermal systems. Geochim Cosmochim Acta 63:627–643

Ehya F (2012) Rare earth element and stable isotope (O, S) geochemistry of barite from the Bijgan deposit, Markazi Province, Iran. Miner Petrol 104:81–93

Elderfield H (1988) The oceanic chemistry of the rare earth elements. Philos Trans R Soc Lond A 325:105–126

Faure G (1998) In U. S. principles and applications of geochemistry. Prentice Hall, New Jersey

Feng D, Roberts HH (2011) Geochemical characteristics of barite deposits at cold seeps from the northern Gulf of Mexico continental slope. Earth Planet Sci Lett. doi:10.1016/j. epsl.2011.06.017

Fuquan Y, Jingwen Y, Yitian W, Frank PB (2006) Geology and geochemistry of the Bulong quartz–barite vein-type gold deposit in the Xinjiang Uygur Autonomous Region, China. Ore Geol Rev 29: 52–76

Ghazban F, McNutt RH, Schwarcz HP (1994) Genesis of sediment-hosted Zn-Pb-Ba deposits in Irankouh, Isfahan area. Econ Geol 89(6):1262–1278

Ghorbani M (2002) An introduction to economic geology of Iran. Natl Geosci Database Iran

Glasby GP, Cherkashov GA, Gavrilenko GM, Rashidov VA, Slovtsov IB (2006) Submarine hydrothermal activity and mineralization on the Kurile and western Aleutian Island arcs. NW Pac Mar Geol 231: 163–180

Göke A, Bozkaya G (2008) Fluid inclusion and stable isotope characteristics of the Karalar (Gazipasa, Antalya) Barite–Galena Deposits, southern Turkey. Geol Ore Depos 50:145–154

Goodfellow WD, Blaise B (1988) Sulfide formation and hydrothermal alteration of hemipelagic sediment in Middle Valley, northern Juan de Fuca Ridge. Can Mineral 26:675–696

Gromet LP, Haskin LA, Korotev RL, Dymek RF (1984) The "North American shale composite": its compilation, major and trace element characteristics. Geochim Cosmochim Acta 48(12):2469–2482

Guichard F, Church TM, Treuil M, Jaffrezic H (1979) Rare earths in barites: distribution and effects on aqueous partitioning. Geochim Cosmochim Acta 49:983–997

Gultekin AH, Orgun Y, Suner F (2003) Geology, mineralogy, and fluid inclusion data of the Kizilcaorenflurite-barite-REE deposit, Eskisehir, Turkey. J Asian Earth Sci 21:365–376

Hall DL, Cohen LH, Schiffman P (1988) Hydrothermal alteration associated with the iron skarn deposit, Eastern Mojave Desert, San Bernardino County. Calif Econ Geol 83:568–587

Hannington MD, Scott SD (1989) Sulfidation equilibria as guides to gold mineralization in volcanogenic massive sulfides; evidence from sulfide mineralogy and the composition of sphalerite. Econ Geol 84(7):1978–1995

Hanor JS (2000) Barite-celestine geochemistry and environments of formation. In: Reviews in mineralogy and geochemistry–sulfate minerals (Eds C.N. Alpers, J.L. Jambor and D.K. Nordstrom), 40, Washington, DC: Mineralogical Society of America

Hedenquist JW, Henlly S, Okay AI (1985) The importance of CO_2 of freezing point measurements of fluid inclusions; evidence from active geothermal system and implications for epithermal ore deposition. Econ Geol 80:1379–1404

Hein JR, Zierenberg RA, Maynard JB, Hannington MD (2007) Multifarious barite-forming environments along a rifted continental margin, southern California Borderland. Deep-Sea Res II 54:1327–1349

Hill GT, Campbell AR, Kyle PR (2000) Geochemistry of southwestern New Mexico fluorite occurrences: implications for precious exploration in fluorite-bearing systems. J Geochem Explor 68:1–20

Hoefs J, Sywall M (1997) Lithium isotope composition of quaternary and tertiary biogene carbonates and a global lithium isotope balance. Geochim Cosmochim Acta 61:2679–2690

Huheey JE, Keiter EA, Keiter RL (1993) Inorganic chemistry: principles of structure and reactivity. Harper-Collins, New York, p 400

Jewell PW, Stallard RF (1991) Geochemistry and paleoceanographic setting of central Nevada bedded barites. J Geol 151–170

Jurković IB, Garašić V, Jurković IM (2011) Geochemical characteristics of mercurian tetrahedrite, barite and fluorite from the Duboki Vagan, Glumac and Dubrave-Dugi Dol barite deposits, south of Kreševo, Mid-Bosnian Schist Mts. Geol Croat 64:49–59

Kesler SE (1977) Geochemistry of Manto barite deposits. Northern Coahuila, Mexico. Econ. Geologija 72:204–218

Klinkhammer G, Elderfield H, Hudson A (1983) Rare earth elements in seawater near hydrothermal vents. Nature 305:185–188

Kusakabe S, Harada K, Mukai T (1990) The rare inversion with a P element at the breakpoint maintained in a natural population of *Drosophila melanogaster*. Genetica 82(2):111–115

Latifi R (2000) Geological, petrological and geochemical study of intrusions in south and northeast of Zaferghand (in Persian). M.Sc thesis, Isfahan University, Iran

Liaghat SM, Moore F, Jami M (2000) Kuh-e-surmeh mineralization: a carbonate-hosted Zn-Pb deposit in the simply folded belt of the Zagros Mountains, SW Iran. Mineral Deposita 35:72–78

Luders V, Pracejus B, Halbach P (2001) Fluid inclusion and sulfur isotope studies in probable modem analogue Kuroko-type ores from the JADE hydrothermal field (Central Okinawa Trough, Japan). Chem Geol 173:45–58

Martin EE, MacDougall JD, Herbert TD, Paytan A, Kastner M (1995) Strontium and neodymium isotopic analyses of marine barite separates. Geochim Cosmochim Acta 59:1353–1361

Maynard JB, Okita PM (1991) Bedded barite deposits in the United States, Canada, Germany, and China; two major types based on tectonic setting. Econ Geol 86(2):364–376

McDonough WF, Sun SS (1995) The composition of the earth. Chem Geol 120:223–253

McLennan SM (1989) Rare earth elements in sedimentary rocks: Influence of provenance and sedimentary processes. In: Lipin BR, McKay GA (eds) Geochemistry and mineralogy of rare earth elements. Rev Mineral 21:169–200

Mohajjel M, Fergusson CL, Sahandi MR (2003) Cretaceous-Tertiary convergence and continental collision, Sanandaj-Sirjan Zone, western Iran. J Asian Earth Sci 21:397–412

Monnin C, Jeandel C, Cattaldo T, Dears F (1999) The marine barite saturation state of the world's oceans. Mar Chem 65:253–261

Murchey BL, Madrid RJ, Poole FG (1987) Paleozoic bedded barite associated with chert in western North America. In: Hein JR (ed) Siliceous sedimentary rock-hosted ores and petroleum. Van Nostrand Reinhold, New York

Murray RW (1994) Chemical criteria to identify the depositional environment of chert: general principles and applications. Sediment Geol 90(3):213–232

Natalin BA, Şengör AM (2005) Late Paleozoic to Triassic evolution of the Turan and Scythian platforms: the pre-history of the Palaeo-Tethyanclosure. Tectonophysics 404:175–202

Noguchi T, Shinjo R, Ito M, Takada J, Oomori T (2011) Barite geochemistry from hydrothermal chimneys of the Okinawa trough: insight into chimney formation and fluid/sediment interaction. J Mineral Petrol Sci 106:26–35

Paytan A, Mearon S, Cobb K, Kastner M (2002) Origin of marine barite deposits: Sr and S isotope characterization. Geology 30(8):747–750

Rees CE, Jenkins WJ, Monster J (1978) The sulphur isotopic composition of ocean water sulphate. Geochim Cosmochim Acta 42(4):377–381

Richards JP, Wilkinson D, Ulrich T (2006) Geology of the sari gunay epithermal gold deposit, Northwest Iran. Econ Geol 101:1455–1496

Roedder E (1984) Fluid inclusions. Rev. Mineral. 12

Ruiz J, Kelley WC, Kaiser CJ (1985) Strontium isotopic evidence for the origin of barites and sulfides from the Mississippi Valley type ore deposits in southeast Missouri- a discussion. Econ Geol 80:773–778

Rushdi AI, McManus J, Collier RW (2000) Marine barite and celestite saturation in seawater. Mar Chem 69:19–31

Seal RR, Alpers CN, Rye RO (2000) Stable isotope systematics of sulfate minerals. Rev Mineral Geochem 40(1):541–602

Shields G, Kimura H, Yang J, Gammon P (2004) Sulphur isotopic evolution of Neoproterozoic-Cambrian seawater: New francolite-bound sulphate $\delta^{34}S$ data and a critical appraisal of the existing record. Chem Geol 204:163–182

Shimizu H, Masuda A (1977) Cerium in chert as an indication of marine environment of its formation. Nature 266:346–348

Stampfli GM (2000) The Tethyan Ocean. In: Bozkurt E, Winchester JA, Piper JDA (eds) Tectonic and magmatism in Turkey and surrounding area, Vol. 173. Geological Society, London, Special Publication, pp 1–23

Stöcklin J (1977) Structural correlation of the Alpine ranges between Iran and central Asia. Mém Hors Sér Soc Géol Fr 8:333–353

Stoffers P, Worthington TJ, Schwarz-Schampera U, Hannington MD, Massoth GJ, Hekinian R, Schmidt M, Lundsten LJ, Evans LJ, Vaiomo'unga R, Kerby T (2006) Submarine volcanoes and high-temperature hydrothermal venting on the Tonga arc, southwest Pacific. Geology 34:453–456

Taghipour B, Moore F, Mackizadeh MA (2010) Stable isotope evidences of jarosite–barite mineralization in the Rangan rhyolitic dome NE Isfahan, Iran. Chem Erde 70:377–384

Torres ME, Bohrmann G, Dube TE, Poole FG (2003) Formation of modern and Paleozoic stratiform barite at cold methane seeps on continental margins. Geology 31:897–900

Valenza K, Moritz R, Mouttaqi A, Fontignie D, Sharp Z (2000) Vein and karst barite deposits in the Western Jebilet of Morocco: fluid inclusion and isotope (S, O, Sr) evidence for regional fluid mixing related to central Atlantic rifting. Econ Geol 95:587–606

Wagner T, Kirnbauer T, Boyce AJ, Fallick AE (2005) Barite–pyrite mineralization of the Wiesbaden thermal spring system, Germany: a 500-kyr record of geochemical evolution. Geofluids 5:124–139

Wang Z, Li G (1991) Barite and witherite deposits in Lower Cambrian shales of South China: stratigraphic distribution and geochemical characterization. Econ Geol 86:354–363

Zhang HF, Li SR, Santosh M, Liu JJ, Diwu CR, Zhang H (2013) Magmatism and metallogeny associated with mantle upwelling: zircon U–Pb and Lu–Hf constraints from the gold-mineralized Jinchang granite, NE China. Ore Geol Rev 54:138–156